

Examination of the Impact of One-Dimensional Crustal Structures on Cascadia Subduction
Zone Earthquake Locations

by
McKenzie Shannon Meyer

A THESIS

submitted to
Oregon State University
Honors College

in partial fulfillment of
the requirements for the
degree of

Honors Baccalaureate of Science in Physics
(Honors Scholar)

Presented May 7, 2020
Commencement June 2020

AN ABSTRACT OF THE THESIS OF

McKenzie Shannon Meyer for the degree of Honors Baccalaureate of Science in Physics presented on May 7, 2020. Title: Examination of the Impact of One-Dimensional Crustal Structures on Cascadia Subduction Zone Earthquake Locations.

Abstract approved: _____

Anne Tréhu

Multiple earthquake events have been recorded off the coast of Oregon, yet their locations have great uncertainty. The largest source of uncertainty is the simple models of the crust that are used to interpret seismic recordings. Because the relationship between earthquake locations and crust are diagnostic of tectonic activity, it is important to determine accurate locations. Knowing how location estimates depend on an assumed crustal structure leads to a better understanding of earthquake activity. Using earthquake waveform data taken in Cascadia, arrival times of seismic waves were used to calculate the locations of three earthquakes. By assuming different crustal structures for the same earthquake, the impact of uncertainties in the structure on location were quantified. One-dimensional crustal structure models were used for three earthquakes: one thick model that had been used previously, and one thin model that better characterizes the crust in Cascadia. The thick crustal structure resulted in deeper earthquake locations while the thin model resulted in shallower locations. Although the thin crustal model resembles the region, the model yields a higher uncertainty than the thick model. While the exact location of the earthquakes is not known, comparing the models has allowed for a better understanding of the uncertainties.

Key Words: earthquake, crustal structure, velocity model, Cascadia, location

Corresponding e-mail address: meyermc@oregonstate.edu

©Copyright by McKenzie Shannon Meyer
May 7, 2020

Examination of the Impact of One-Dimensional Crustal Structures on Cascadia Subduction
Zone Earthquake Locations

by
McKenzie Shannon Meyer

A THESIS

submitted to
Oregon State University
Honors College

in partial fulfillment of
the requirements for the
degree of

Honors Baccalaureate of Science in Physics
(Honors Scholar)

Presented May 7, 2020
Commencement June 2020

Honors Baccalaureate of Science in Physics project of McKenzie Shannon Meyer presented on May 7, 2020.

APPROVED:

Anne Tréhu, Mentor, representing Geology and Geophysics

Robert Harris, Committee Member, representing Geology and Geophysics

Randall Milstein Committee Member, representing Physics

Toni Doolen, Dean, Oregon State University Honors College

I understand that my project will become part of the permanent collection of Oregon State University, Honors College. My signature below authorizes release of my project to any reader upon request.

McKenzie Shannon Meyer, Author

I would like to thank the Research Experience for Undergraduates (REU) program at the College of Earth, Ocean, and Atmospheric Sciences at Oregon State University (OSU) for accepting me into the program. I also thank Kaplan Yalcin for leading the REU program and providing memorable times and tons of resources to help us grow as researchers. I would like to thank the National Science Foundation for funding this program. Finally, I would like to thank my mentor, Anne Tréhu, and her post doc, Kathy Davenport, for guiding and supporting me through my research project, both in the REU program and through the process of my senior thesis.

Table of Contents

List of Figures.....	3
Chapter 1 – Introduction.....	7
1.1 Summary.....	7
1.2 Background.....	7
Chapter 2 – Methods.....	11
Chapter 3 – Results.....	16
3.1 Stations.....	16
3.2 June 28, 2012 Event.....	16
3.3 June 30, 2012 Event.....	20
3.4 June 21, 2012 Event.....	23
Chapter 4 – Discussion and Conclusion.....	29
Chapter 5 – Future Research.....	35
References.....	36
Appendix: Tables.....	37
Table 1.....	37
Table 2.....	39
Table 3.....	41
Table 4.....	41
Table 5.....	43
Table 6.....	44
Table 7.....	45
Table 8.....	46

Table 9.....	47
Table 10.....	49
Table 11.....	49

List of Figures

- Figure 1: Example of a slice of the crust of the Juan de Fuca plate in the Cascadia Subduction Zone. The color bar shows the velocity of P-waves traveling through the crust. Notable rock types are listed on large sections of the same color. The black vertical line on the right shows, approximately, the slice of crust that PNSN assumes for everywhere in the region for their thick crustal model. The black line on the left shows, approximately, the slice of crust for the thin model, derived from the air gun shots. Adapted from ref. [6]...9
- Figure 2: Waveform data from the June 30, 2012 event from onshore station 1 in PQL II software. The horizontal axis for all of the data is time and the vertical component is a unitless amplitude. The bottom red X is on the vertical component of the data and is the pick for the P-wave arrival time, which also has an up polarity. The top red X is on the East-West component of the data and is the pick for the S-wave arrival time.....12
- Figure 3: Map of temporary stations used in this experiment on and off the coast of Oregon. Map made using GeoMapApp 3.6.10.0.....14
- Figure 4: Difference between S- and P-wave arrival times versus P-wave arrival time for the June 28, 2012 event, relative to 19:35. Blue dots are data from land stations. Red dots are data from OBSs.....17
- Figure 5: Map of possible earthquake locations from HYPO71 based off the different crustal models and values for V_p/V_s ratio. Each circle is a possible location for the June 28,

2012 event based on the parameters listed in the legend. All stations are used except for OR13 and OR50. Map made using GeoMapApp 3.6.10.0.....18

Figure 6: Map of possible earthquake locations from HYPO71 based off the different crustal models and values for V_p/V_s ratio. Each circle is a possible location for the June 28, 2012 event based on the parameters listed in the legend. All of the on-shore stations are used, except for OR13, and none of the off-shore station data are used. Map made using GeoMapApp 3.6.10.0.....19

Figure 7: Difference between S- and P-wave arrival times versus P-wave arrival time for the June 30, 2012 event, relative to 16:43. Blue dots are data from land stations. Red dots are data from OBSs.....20

Figure 8: Map of possible earthquake locations from HYPO71 based off the different crustal models and values for V_p/V_s ratio. Each circle is a possible location for the June 30, 2012 event based on the parameters listed in the legend. All stations are used except for OR09. Map made using GeoMapApp 3.6.10.0.....21

Figure 9: Map of possible earthquake locations from HYPO71 based off the different crustal models and values for V_p/V_s ratio. Each circle is a possible location for the June 30, 2012 event based on the parameters listed in the legend. All of the on-shore stations are used, except for OR09, and none of the off-shore station data are used. Map made using GeoMapApp 3.6.10.0.....22

- Figure 10: Difference between S- and P-wave arrival times versus P-wave arrival time for the June 21, 2012 event, relative to 15:57.....23
- Figure 11: Map of possible earthquake locations from HYPO71 based off the different crustal models and values for V_p/V_s ratio. Each circle is a possible location for the June 21, 2012 event based on the parameters listed in the legend. All of the available stations are used, except for OR20. Map made using GeoMapApp 3.6.10.0.....24
- Figure 12: Map of specifically chosen stations to test their data together for the June 21, 2012 earthquake location. The stations were chosen by being the farthest in each cardinal direction, plus two from the middle of the network of stations. The stations are OR01, OR11, OR15, OR30, OR32, and OR54. Map made using GeoMapApp 3.6.10.0.....25
- Figure 13: Map of possible earthquake location for June 21, 2012 from HYPO71 using the PNSN crustal model and 1.78 V_p/V_s ratio. The stations used are depicted in Figure 12. Map made using GeoMapApp 3.6.10.0.....26
- Figure 14: Map of current PNSN stations, as of 2018.....27
- Figure 15: Map of stations chosen to replicate the current PNSN stations that are active. The stations are OR04, OR05, OR06, OR07, OR08, OR09, OR10, OR11, OR14, OR16, OR17, OR18, OR21, OR25, OR27, OR28, OR29, and OR30. Mapped using GeoMapApp 3.6.10.0.....27

Figure 16: Map of possible earthquake location for June 21, 2012 from HYPO71 using the PNSN crustal model and 1.78 V_p/V_s ratio. The stations used are depicted in Figure 15.

Mapped using GeoMapApp 3.6.10.0.....28

Chapter 1 – Introduction

1.1 Summary

Current earthquake location methods are plagued with large uncertainty. The formal uncertainty of an earthquake location changes with the assumed P-wave travel velocity model for the crust used to obtain the location. Currently, simple crustal structures and velocity models are used because they roughly match the average velocities observed in seismic measurements for a large area. However, the uncertainty of the earthquake locations can be very high in certain smaller regions when this simplified velocity model does not reflect the actual crustal structure. The goal of this project is to take earthquake waveform data from seismometers in the Cascadia Subduction Zone and derive a more exact location for each earthquake by using a more realistic Earth model for the region. The significance of this project is that we will better locate earthquakes in this region, which can help describe how they develop and behave, while also learning about the uncertainties between velocity models and how these uncertainties affect the derived earthquake locations.

1.2 Background

Cascadia has a relatively low number of instrumentally recorded seismic activity to use even though it is a highly active area [1], which speaks to the challenges of obtaining earthquake data. One of the first challenges encountered is recording seismic waves offshore [2], where most earthquakes occur. Seismometers record seismic waves in three orthogonal components of the ground motion [2] (one vertical and two horizontal) that record well onshore but prove to be difficult in the ocean with the low shear strength of marine sediments and interference from

ocean waves [3] and sea life [2]. The general distribution of all seismometers, on and offshore, can also cause problems with recording seismic waves because biases with latitude and longitude can appear in earthquake data if the distribution is not equal around the earthquake [2]. Though there are challenges associated with obtaining earthquake data, the ever-evolving technology and techniques are paired with velocity models to derive locations for earthquakes in regions like Cascadia.

Pacific Northwest Seismic Network (PNSN) is one example of a network that tracks, records, and analyzes the seismic activity occurring in Cascadia. PNSN records waveform data from earthquakes on a network of seismometers in the region. From the waveform data, PNSN also derives the location of the earthquakes using simple Earth models of their own. The simple models give a good estimate to where earthquakes are located in plane with the surface of the Earth; however, the estimated depth has a large uncertainty [4]. To develop a more accurate velocity model, earthquake data can be simulated using controlled air gun shots from research vessels. These act like earthquakes because the air gun shots behave as seismic waves would through the crust. By recording these air gun shots with the same onshore and offshore seismometers that record the earthquakes, a better velocity model for the specific region can be derived. Earth structure models are then fit to the derived velocity model to complete a more complicated and accurate picture of what the structure of the Earth is for that region.

Although the calculations take longer than with the simple models [5], the significance of using more complicated models is that the models lead to more precise earthquake locations with smaller uncertainties. Additionally, past analysis of earthquakes in the Cascadia Subduction Zone specifically have indicated that the local geometry is complex, calling for a much more

accurate and complex model than simple ones like PNSN's [1]. Figure 1 illustrates the difference in thickness between PNSN model and the thin model derived from air gun shots by slicing a two-dimensional velocity profile of the Juan de Fuca plate into two one-dimensional lines for each of two models used here, with the PNSN model assuming that the subduction Juan de Fuca plate is deeper than the thin model assumes.

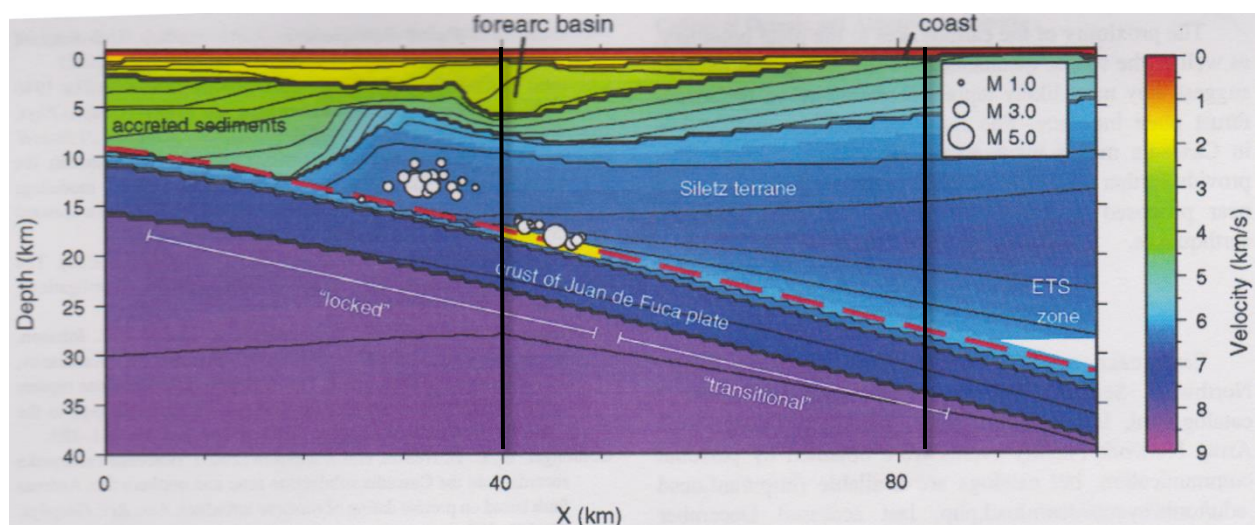


Figure 1: Example of a slice of the crust of the Juan de Fuca plate in the Cascadia Subduction Zone. The color bar shows the velocity of P-waves traveling through the crust. Notable rock types are listed on large sections of the same color. The black vertical line on the right shows, approximately, the slice of crust that PNSN assumes for everywhere in the region for their thick crustal model. The black line on the left shows, approximately, the slice of crust for the thin model, derived from the air gun shots. Adapted from ref. [6].

Complicated models have been used in the past to relocate earthquakes in Cascadia [4,6]; therefore, we will further examine this correlation between velocity model and uncertainty of

earthquake location in Cascadia, while finding better locations for more earthquake events, both with the PNSN and air-gun-shot-derived velocity models. Knowing more accurate locations for these earthquakes leads to better understanding the tectonic implications of the earthquakes and the behavior of the subduction zone [2].

We expect to derive earthquake locations from HYPO71 similar to the locations from PNSN when looking in the plane with the Earth surface (latitude and longitude), but with shallower depth in the vertical direction [6]. We also expect the uncertainty (root-mean-square) of our calculated earthquake locations to be smaller compared to PNSN's locations.

Chapter 2 – Methods

Working with Dr. Anne Tréhu, we used inverse theory to derive earthquake locations [7] for three earthquakes in Cascadia using one-dimensional velocity models. Inverse theory is the method of calculating a starting event by looking at many ending observables and back-tracking to the original source. Using waveform data from the Incorporated Research Institutions for Seismology (IRIS) database, we picked the times at which the earthquake waveforms were recorded. The earthquake waveform data we looked at were recorded on seismometers onshore and offshore the coast of Oregon in June of 2012. We started by hand-picking the specific times that the pressure and shear waves (P- and S-waves) arrived at the different onshore and offshore stations near each earthquake using PQL II software, a software created by IRIS to view time-series data. To pick the arrival time of the P-wave for a set of waveform data within PQL II, the vertical component of the waveform data was examined manually for the earthquake motion. The exact time of arrival was then given by the software. We also noted the polarity of the P-wave arrival to tell us more about direction of slip on the fault plane for these earthquakes. The polarity was determined by whether the P-wave first traveled up or down after the initial arrival time in PQL II. The arrival time of the S-wave was picked in the same fashion as the P-wave but the horizontal components were examined. An example of the waveform data picking software is shown in Figure 2.

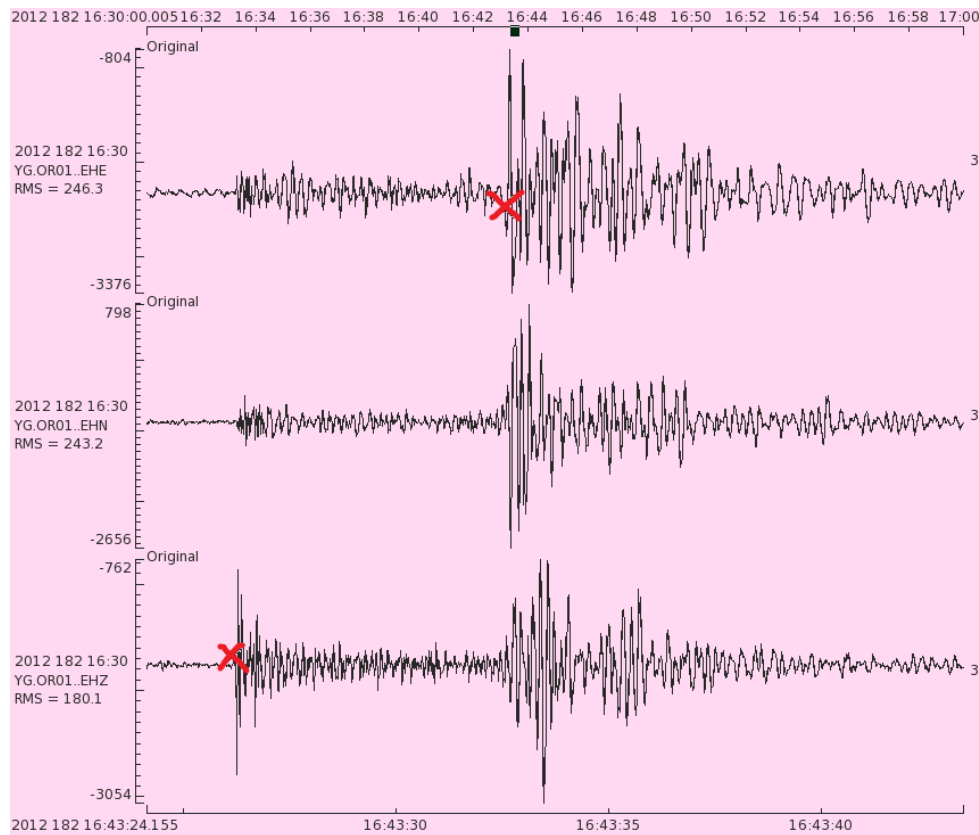


Figure 2: Waveform data from the June 30, 2012 event from onshore station 1 in PQL II software. The horizontal axis for all of the data is time and the vertical component is a unitless amplitude. The bottom red X is on the vertical component of the data and is the pick for the P-wave arrival time, which also has an up polarity. The top red X is on the East-West component of the data and is the pick for the S-wave arrival time.

With these picked times of P- and S-wave arrivals, we were able to determine another important parameter in finding the earthquake locations: the ratio of the velocity of P-waves to the velocity of S-waves (V_p/V_s ratio). The V_p/V_s ratio was found for each earthquake by calculating the difference between S- and P-wave arrival times for each station and plotting those times versus the P-wave arrival time of each station. The slope of the trendline line of this graph plus one is

the calculated V_p/V_s ratio of the earthquake. This ratio is reasonably independent of location for the area of Earth we were examining; therefore, no matter where we assumed the earthquake was, the V_p/V_s ratio remained constant for all three events. Furthermore, the graph that was used to find the V_p/V_s ratio was used as a quality check for the data. If the data agreed with the trendline, the picks were accurate while outliers on the graph were examined for problems with picking and/or the station itself.

In addition to knowing the earthquake arrival times, we needed to know information about the stations themselves to understand where an earthquake originated and the direction it traveled to a specific station. The station locations in this network are already known (as shown in Figure 3), are characterized by its latitude, longitude and elevation, but each station had a delay time relative to its elevation. For each station, the elevation was divided by the average speed of seismic waves in their respective medium to find this time delay.

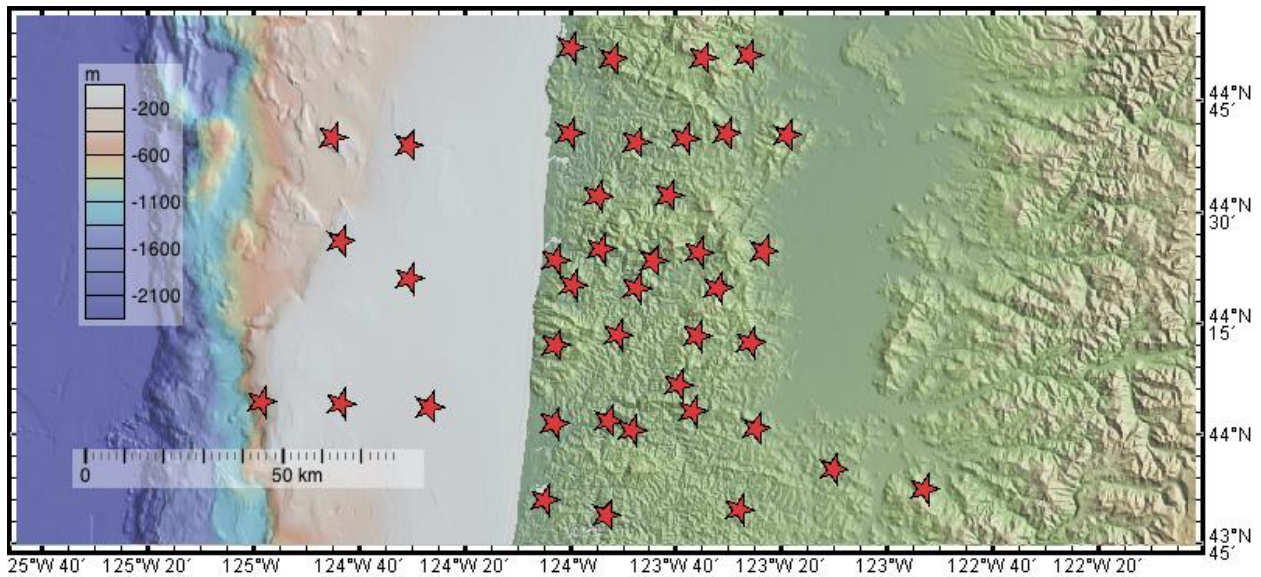


Figure 3: Map of temporary stations used in this experiment on and off the coast of Oregon.

Map made using GeoMapApp 3.6.10.0.

With the picked times, P-wave polarities, V_p/V_s ratios, station locations, and station delay times, we ran the data through HYPO71 software to derive locations for earthquakes with the Earth crustal model derived from air gun shots. HYPO71 calculates the hypocenter, magnitude, and the first motion of earthquakes, though we use it here for obtaining the hypocenter. Different combinations of other unknown parameters were tested in HYPO71 including different V_p/V_s ratios. Even though we calculated the most realistic V_p/V_s ratio based on the picked arrival times, we also tested three other ratio values that fall in the range of common ratios for this area. With all of these parameters and data, HYPO71 gave a location for the earthquake, along with its uncertainty including the root-mean-square uncertainty and other useful information about the event. We also examined how these derived locations compared to PNSN's locations by running PNSN's crustal model through HYPO71. Additionally, we examined how the presence or absence of offshore stations affected the earthquake locations by excluding offshore station data

from the HYPO71 data, along with testing other combinations of onshore and offshore stations.

To visualize the different locations that all these parameters gave, we mapped the locations using

GeoMapApp 3.6.10.0.

Chapter 3 – Results

3.1 Stations

The known station data, such as the location and elevation, along with the calculated station delay times, was used for all three earthquake events and is recorded in Table 1 (all tabulated data can be found in the Appendix). The station delay times were calculated using 2.5 km/s for seismic waves through the crust in this region and 1.5 km/s for seismic waves through water.

3.2 June 28, 2012 Event

The first earthquake event we looked at occurred on June 28, 2012. Table 2 records the picks from this first event along with the difference between the S- and P-wave arrival times used to find the V_p/V_s ratio in the graph depicted in Figure 4. Not all stations were able to be picked due to noise.

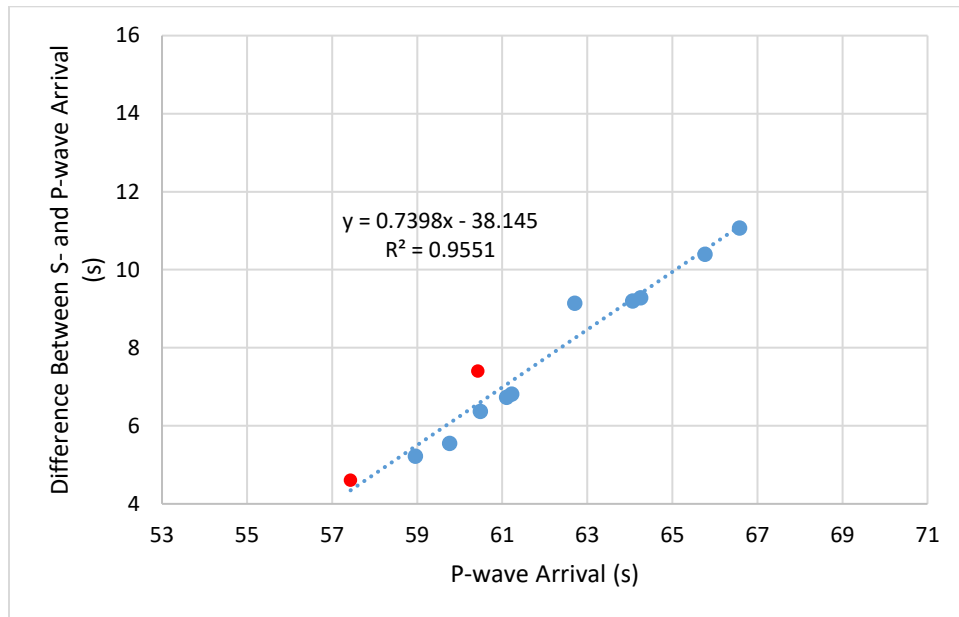


Figure 4: Difference between S- and P-wave arrival times versus P-wave arrival time for the June 28, 2012 event, relative to 19:35. Blue dots are data from land stations. Red dots are data from OBSs.

From Figure 4, the calculated V_p/V_s ratio for the June 28, 2012 event was 1.74.

Running all of the data collected in Tables 1 and 2 through HYPO71 yields the results that are recorded in Table 3 and mapped in Figure 5. Stations OR13 and OR50 were removed from the data due to evidence of problems with the station itself at the time of the earthquake.

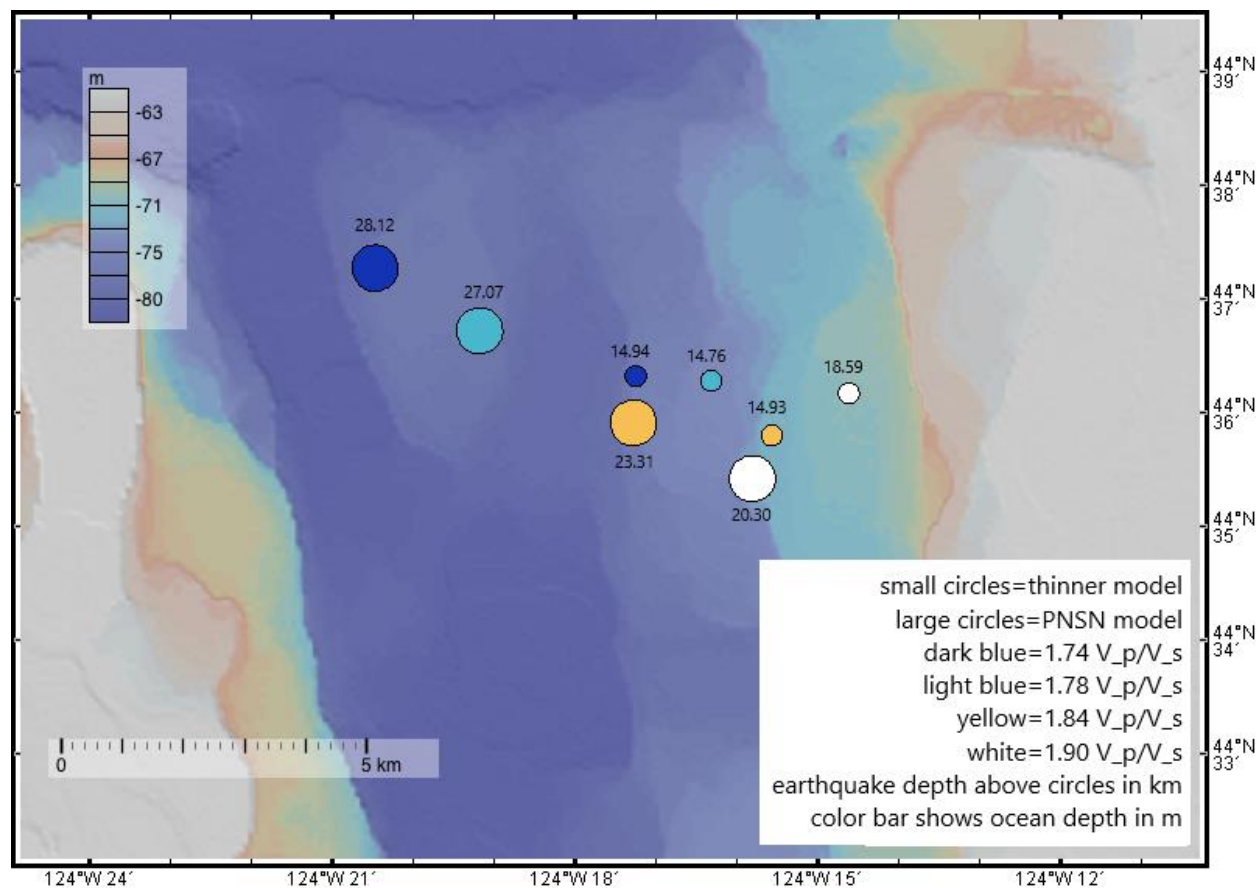


Figure 5: Map of possible earthquake locations from HYPO71 based off the different crustal models and values for V_p/V_s ratio. Each circle is a possible location for the June 28, 2012 event based on the parameters listed in the legend. All stations are used except for OR13 and OR50. Map made using GeoMapApp 3.6.10.0.

Running data for the June 28, 2012 event using only the on-shore stations, and leaving out the OBS data, yields results from HYPO71 recorded in Table 4 and a map of the locations in Figure 6. Station OR13 was left out again as well.

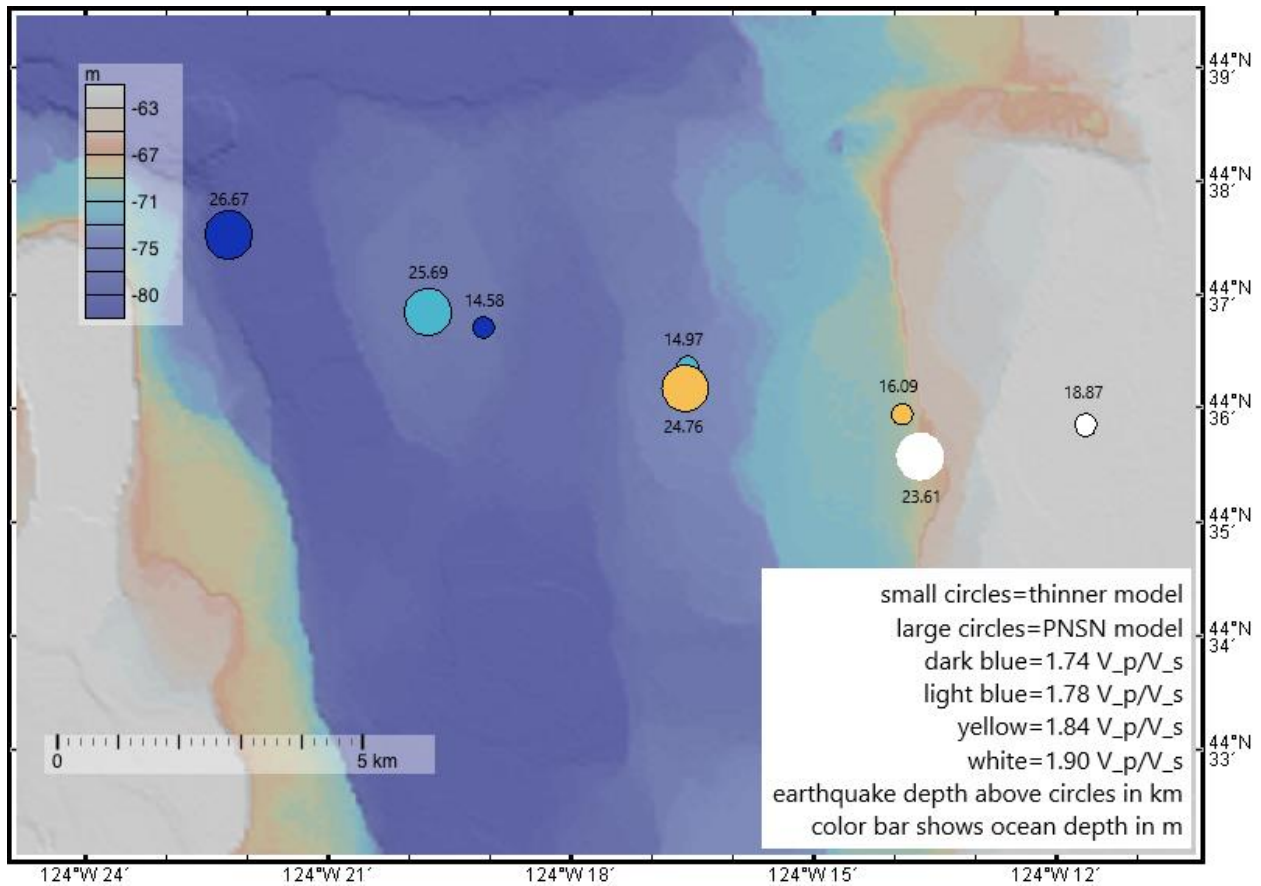


Figure 6: Map of possible earthquake locations from HYPO71 based off the different crustal models and values for V_p/V_s ratio. Each circle is a possible location for the June 28, 2012 event based on the parameters listed in the legend. All of the on-shore stations are used, except for OR13, and none of the off-shore station data are used. Map made using GeoMapApp 3.6.10.0.

In both Figures 5 and 6, the PNSN model yields deeper earthquake depths than the thin model. Additionally, the PNSN model has a wider range in depth values than the thin model for data with OBSs in Figure 5, but has a smaller range of depth values in Figure 6 without OBSs. Furthermore, the hypocenters in Figure 6 were spread out across the map more than those in Figure 5.

3.3 June 30, 2012 Event

The second earthquake event we looked at occurred on June 30, 2012. Table 5 records the picks from this second event along with the difference between the S- and P-wave arrival times used to find the V_p/V_s ratio in the graph depicted in Figure 7. Not all stations were able to be picked well due to noise.

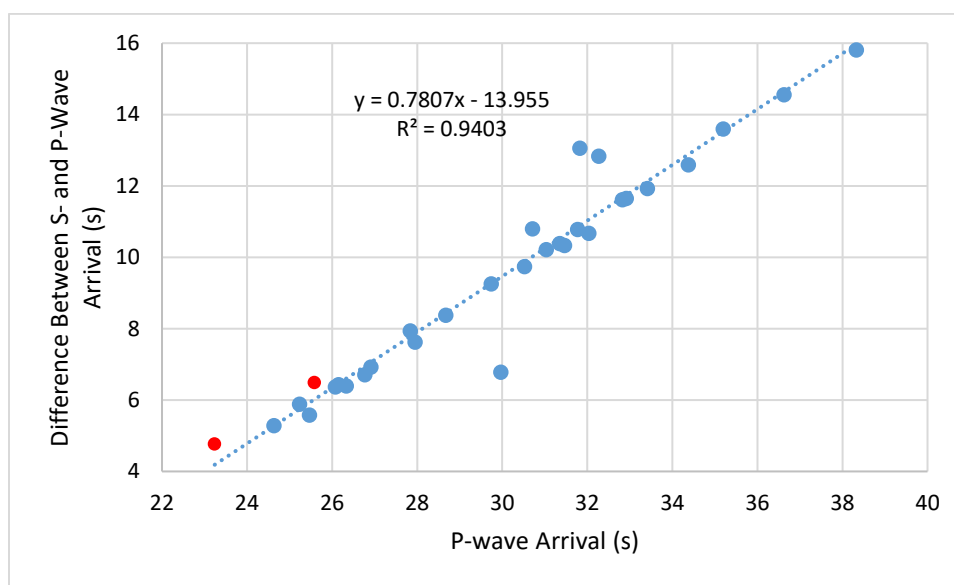


Figure 7: Difference between S- and P-wave arrival times versus P-wave arrival time for the June 30, 2012 event, relative to 16:43. Blue dots are data from land stations. Red dots are data from OBSs.

From Figure 7, the calculated V_p/V_s ratio for the June 30, 2012 event was 1.78.

Running all of the data collected in Tables 1 and 5 through HYPO71 yields the results that are recorded in Table 6 and depicted in Figure 8. Station OR09 was left out of the data because, when it was included, its data was flagged as an outlier on every single run by HYPO71.

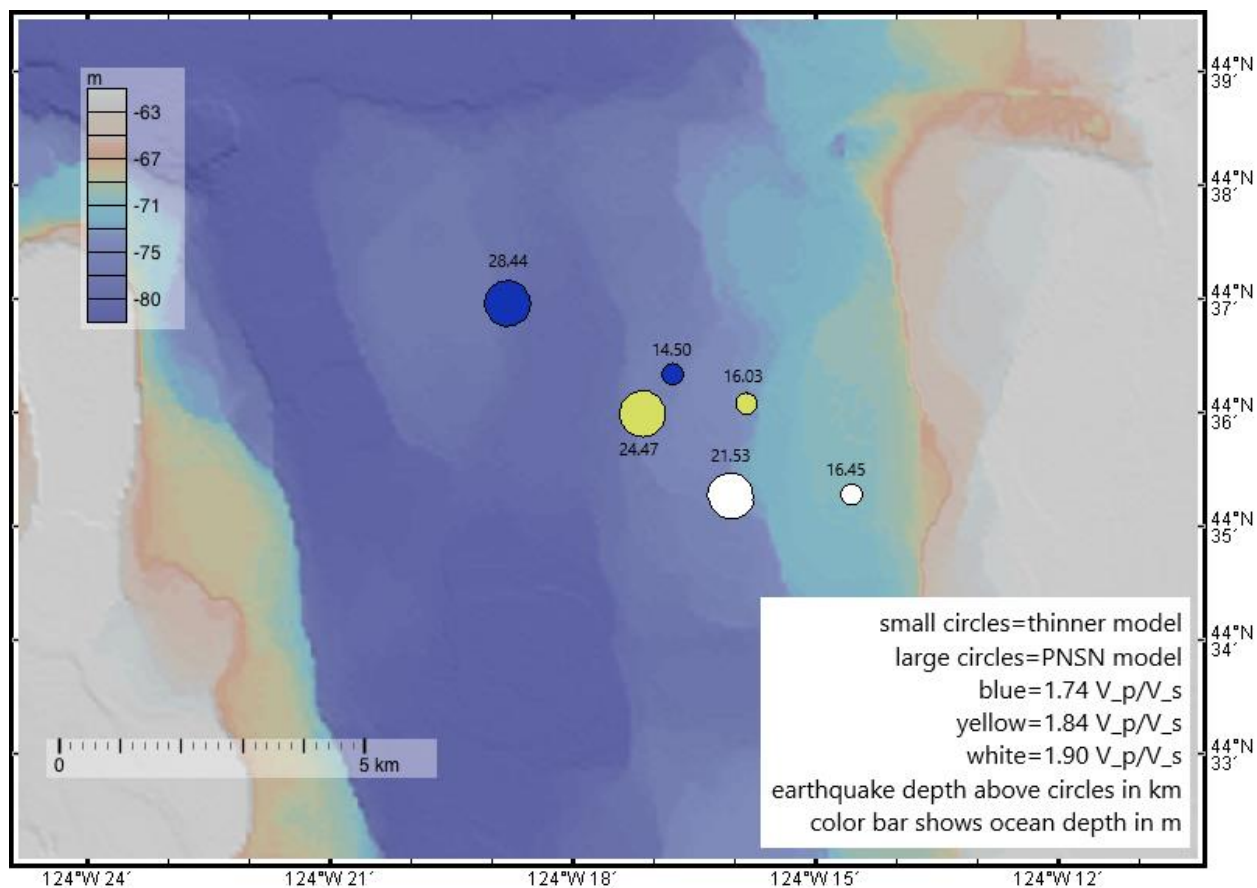


Figure 8: Map of possible earthquake locations from HYPO71 based off the different crustal models and values for V_p/V_s ratio. Each circle is a possible location for the June 30, 2012 event based on the parameters listed in the legend. All stations are used except for OR09. Map made using GeoMapApp 3.6.10.0.

Running data for the June 30, 2012 event using only the on-shore stations, and leaving out the OBS data, yields results from HYPO71 recorded in Table 7 and a map of the locations in Figure 9. Station OR09 was left out again as well.

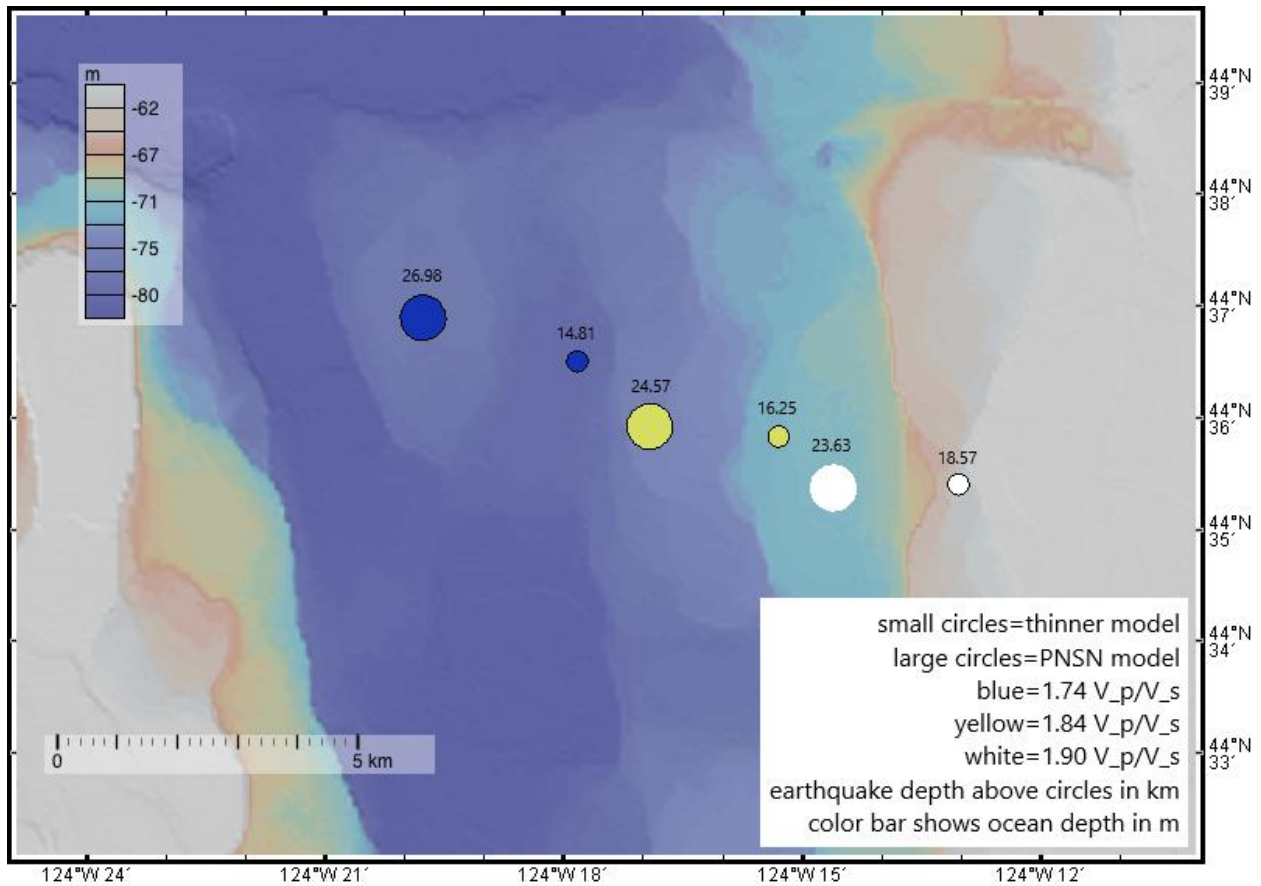


Figure 9: Map of possible earthquake locations from HYPO71 based off the different crustal models and values for V_p/V_s ratio. Each circle is a possible location for the June 30, 2012 event based on the parameters listed in the legend. All of the on-shore stations are used, except for OR09, and none of the off-shore station data are used. Map made using GeoMapApp 3.6.10.0.

In both Figures 8 and 9, the PNSN model yields deeper earthquake depths than the thin model. Additionally, the PNSN model has a wider range in depth values than the thin model for data with OBSs in Figure 8, but has a smaller range of depth values in Figure 9 without OBSs. Furthermore, the hypocenters in Figure 9 were spread out across the map more than those in Figure 8.

3.4 June 21, 2012 Event

The final earthquake event we looked at occurred on June 21, 2012. Table 8 records the picks from this final event along with the difference between the S- and P-wave arrival times used to find the V_p/V_s ratio in the graph depicted in Figure 10. Not all stations were able to be picked from fully due to high noise volume and the event being further South than the first two events. None of the OBSs picked up this event so only land stations were used, of which only about half picked up the event.

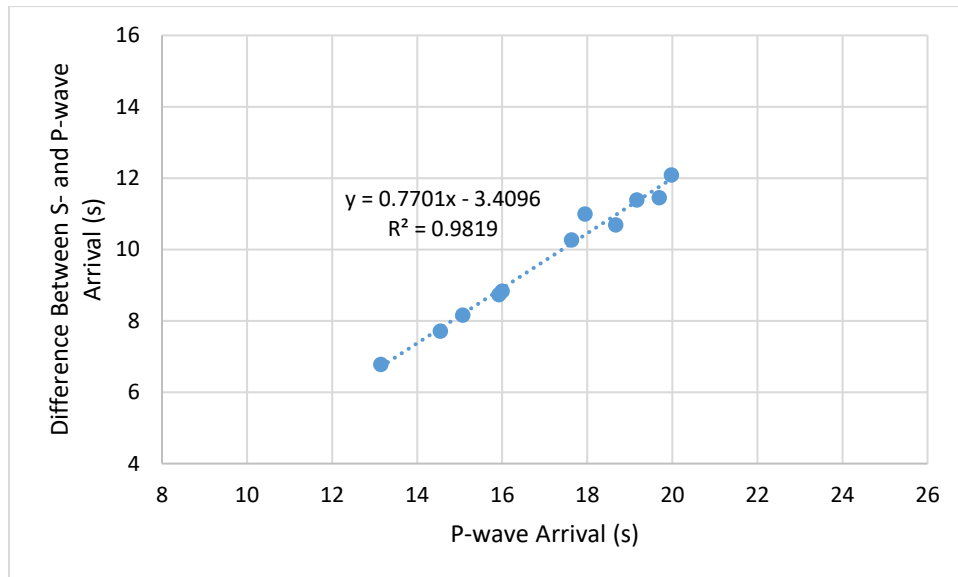


Figure 10: Difference between S- and P-wave arrival times versus P-wave arrival time for the June 21, 2012 event, relative to 15:57.

From Figure 10, the calculated V_p/V_s ratio for the June 21, 2012 event was 1.77.

Running all of the data collected in Tables 1 and 8 through HYPO71 yields the results that are recorded in Table 9 and depicted in Figure 11. Station OR20 was left out of the data because, when it was included, its data is an outlier on every single run.

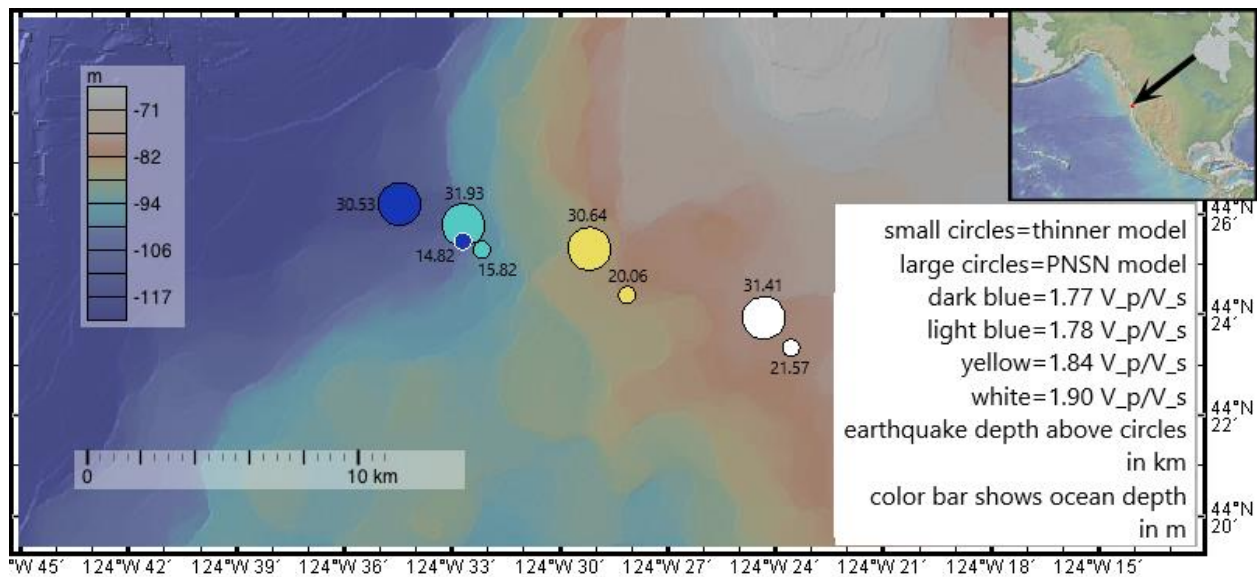


Figure 11: Map of possible earthquake locations from HYPO71 based off the different crustal models and values for V_p/V_s ratio. Each circle is a possible location for the June 21, 2012 event based on the parameters listed in the legend. All of the available stations are used, except for OR20. Map made using GeoMapApp 3.6.10.0.

In Figure 11, the PNSN model yields deeper earthquake depths than the thin model while also having a smaller range in depth values than the thin model.

For the June 21, 2012 event, we also tested different combinations of data from specific stations. The first combination of stations tested were ones that were the farthest in each cardinal direction, plus a couple in the middle, mapped in Figure 12.

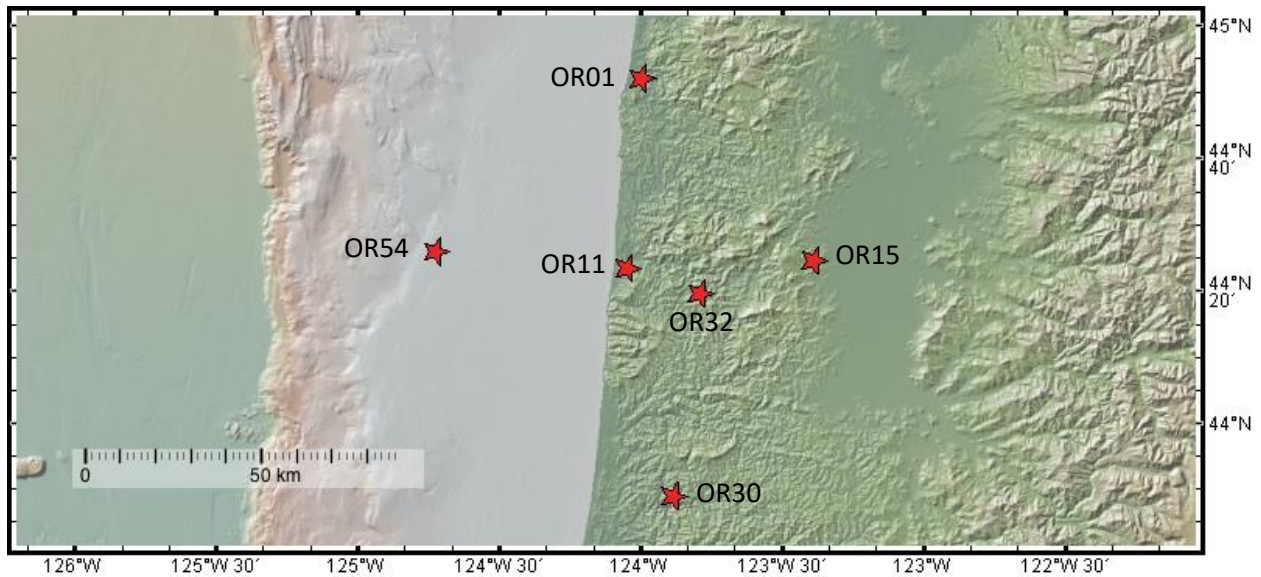


Figure 12: Map of specifically chosen stations to test their data together for the June 21, 2012 earthquake location. The stations were chosen by being the farthest in each cardinal direction, plus two from the middle of the network of stations. The stations are OR01, OR11, OR15, OR30, OR32, and OR54. Map made using GeoMapApp 3.6.10.0.

Table 10 records the results from HYPO71 for the combination of stations depicted in Figure 12. Only one crustal model (PNSN) and V_p/V_s ratio (1.78) was tested. The location is mapped in Figure 13.

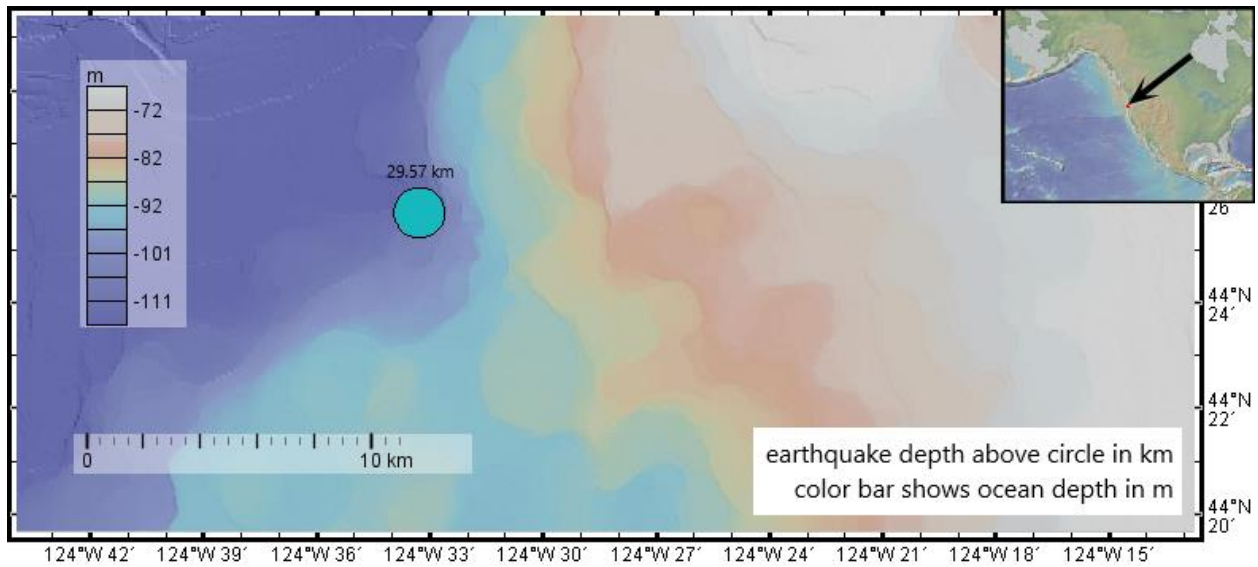


Figure 13: Map of possible earthquake location for June 21, 2012 from HYPO71 using the PNSN crustal model and 1.78 V_p/V_s ratio. The stations used are depicted in Figure 12. Map made using GeoMapApp 3.6.10.0.

The second combination of stations tested with the June 21, 2012 event was replicating PNSN's current network of stations. Figure 14 maps the current PNSN stations, as of 2018, which we tried to replicate in Figure 15 with our network of stations.



Figure 14: Map of current PNSN stations, as of 2018.

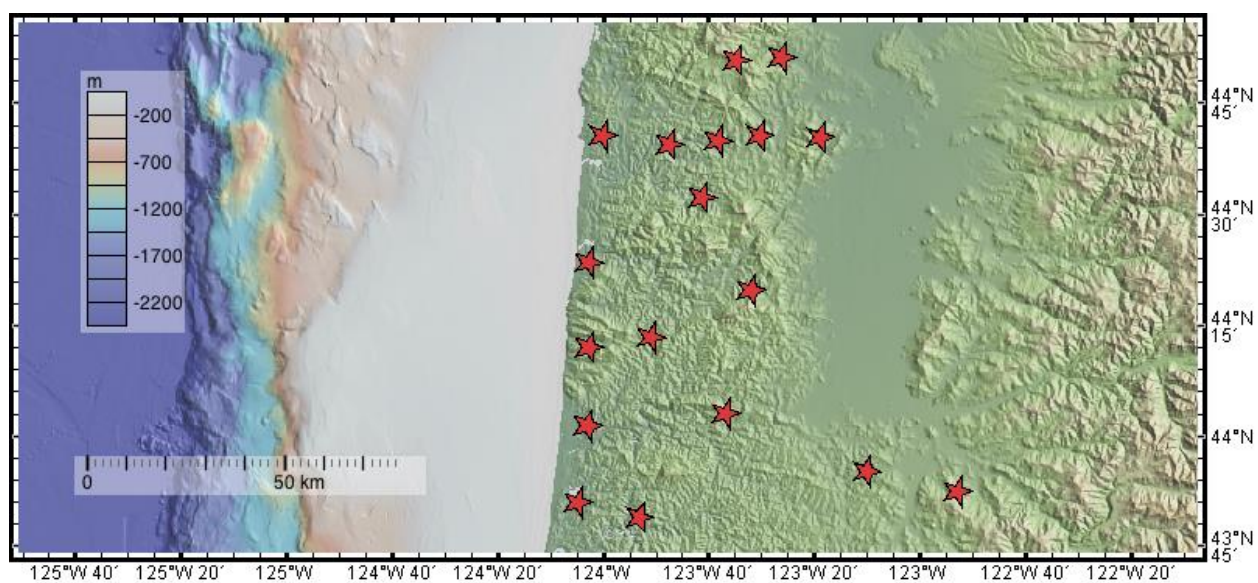


Figure 15: Map of stations chosen to replicate the current PNSN stations that are active. The stations are OR04, OR05, OR06, OR07, OR08, OR09, OR10, OR11, OR14, OR16, OR17, OR18, OR21, OR25, OR27, OR28, OR29, and OR30. Mapped using GeoMapApp 3.6.10.0.

Table 11 records the results from HYPO71 for the combination of stations depicted in Figure 15. Only one crustal model (PNSN) and V_p/V_s ratio (1.78) was tested. The location is mapped in Figure 16.

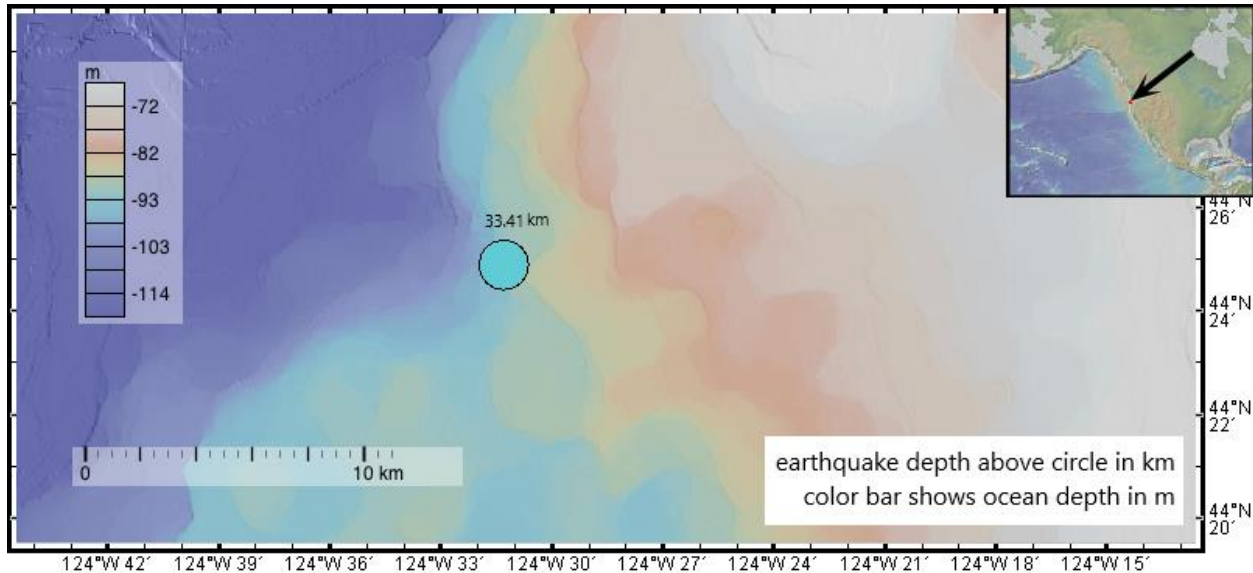


Figure 16: Map of possible earthquake location for June 21, 2012 from HYPO71 using the PNSN crustal model and 1.78 V_p/V_s ratio. The stations used are depicted in Figure 15. Mapped using GeoMapApp 3.6.10.0.

The other two earthquake events were tested with these two different station combinations; however, HYPO71 was including extra stations in the data not mapped in Figures 12 and 15, for their respective combinations, giving results for station combinations we did not want.

Chapter 4 – Discussion and Conclusion

In this thesis, we explored the uncertainty and potential bias in earthquake hypocenters for earthquakes located on the continental margin offshore Oregon. In particular, we explored the effects of assuming two different one-dimensional velocity models (referred to as thick crust and thin crust), four different V_p/V_s ratios, and station distributions that included or did not include offshore stations. Testing these different scenarios provided insights into the relative importance of different sources of uncertainty, including errors in picking the arrival times from waveforms, errors in the timing base of the seismometers, errors in the velocity model assumed when locating the earthquakes, and errors due to the spatial distribution of the observations.

The first conclusion drawn from the results supports what has been shown in other papers (e.g., Williams et al., 2011 [6]); the hypocentral depths determined with the thick crust model are deeper than those obtained with the thin crustal model. The average earthquake depth for the thick crust model across all three earthquake events is 26.8 km (3.5 km standard deviation), while the thin crust model has an average depth of 16.5 km (2.1 km standard deviation). Another observation is that, with the thick crust model, the depths are spread out over a wide range for the different V_p/V_s ratios, while the thin crust model yields depth values that are less sensitive to the assumed V_p/V_s ratio. Given that the thin crust model has more consistent depths over a wide range of ratios, this observation is consistent with the conclusion of Williams et al. [6]: depths obtained by using the thin crust model are more accurate than those obtained with the thick crust model. However, this observation only holds when OBS data are included. When OBS data are excluded, the thin crust model keeps a consistent range in depth while the thick crust model shrinks in depth range, suggesting that the results from the thick crust model are greatly

influenced by OBS data since the OBS stations were not in the region represented by the thick crust model.

The rest of the conclusions drawn from this project are based on the uncertainty values of the earthquake locations. Because the primary input data for calculating an earthquake location are the observed arrival times of P- and S-waves at seismic stations, an important measure of the uncertainty of a hypocenter solution is the root-mean-square (RMS) value of the misfit between the predicted and observed arrival times. While picking arrival times, measurement precision and measurement accuracy both contribute to the RMS values. Precision is the repeatability of multiple attempts to pick arrival times from a particular waveform and is affected by actions such as having various zoom window sizes for picking and determining the difference between background seismic noise and an earthquake. Over time, as I gained experience, my picks became more consistent due to corrections such as zooming into the earthquake arrival point the same amount for each station and recognizing the behavior of an earthquake wave versus background noise. On the other hand, accuracy is the closeness of the measurements to the actual value and is affected by aspects of the stations themselves such as the stations' internal clocks and whether they were synchronized with GPS. The RMS values take into account both the precision and accuracy of the measurements, but since I was able to measure more precisely as the project went on, as well as go back and revise my less-precise earlier picks, the RMS value is mostly affected by the accuracy of the seismometers, a factor over which we had no control. The RMS values are included in the tables in the Appendix.

Although neither of the one-dimensional velocity models used in this project accurately represents the velocity structure within the entire three-dimensional volume within which the

seismic waves traveled, they provide a good estimate for different slices of the region. Despite knowing the thin crust model to be more accurate for the offshore region (where the earthquakes are located) since this model was derived from air gun shots in this specific region, the RMS values for the thick crust model are lower than those for the thin crust model. This unexpected result can be attributed to the fact that the RMS values are affected by the accuracy of the stations. While we know the earthquakes are located within the region characterized by the thin crust model, the majority of the stations are on land and in a region well characterized by the thick crust model (Figure 1), creating a bias towards the land and resulting in a lower RMS value for the earthquake locations even though the earthquakes are not in a thick region of the crust.

There was also an unexpected RMS value associated with the number of stations used. When more stations were used, the RMS was higher when, generally, it should decrease as more data contribute to the results. The observation of a higher RMS with more stations indicates that we potentially had poor data being added to the calculations that did not match any other data in the set. For example, when looking at the difference in RMS values when using the OBS data versus not using OBS data, using the OBS data resulted in a higher RMS than without it. We know that OBS data are prone to being noisier and more inaccurate than land stations due to factors of the ocean environment. The first effect from the marine environment on the OBSs is the possibility for the internal clock to drift from the actual time since GPS does not work underwater. Secondly, there is greater uncertainty due to the shallow sediment velocity the OBSs are positioned on. And lastly, the background noise level is higher due to ocean waves and marine life. On top of the general uncertainty of the OBSs from their marine environment, there are significantly fewer OBS stations than land stations, which can bias the solution that

includes OBS data if even just one offshore seismometer has significant errors. On the other hand, there was an observation when comparing results with and without OBS data that lead to the conclusion that more stations were better, even if they potentially had poorer quality. When looking again at the maps with OBS data versus without OBS data, the spread of epicenters was much greater without OBS data than with it. With the OBS data, the potential hypocenters were much closer together, leading to a smaller volume within which the earthquake could have happened. Without the OBS data, the potential source volume for the earthquake is much larger.

Finally, the RMS value is lower for all of the earthquakes when a V_p/V_s ratio of 1.78 is assumed. This observation leads us to conclude that 1.78 is the most accurate V_p/V_s ratio to use for locating earthquake in this region. This value is also supported by the difference between S- and P-wave arrival times versus P-wave arrival time plots, which are independent of the assumed crustal model. All of the graphs produced ratio values that were within 0.04 units of the 1.78 value, with the June 30th earthquake having a calculated value of exactly 1.78. These three earthquakes were recorded by an unusually large number of stations because they occurred during a controlled source experiment when an exceptionally large number of temporary stations were on the ground. This large number of closely spaced observations permitted a particularly well-constrained determination of the 1.78 V_p/V_s ratio.

The other uncertainty values examined are the formal errors, both in the horizontal and vertical directions. These two error values are based off of what HYPO71 calculates these uncertainties to be based on the RMS misfit and geometrical factors that take into account the inhomogeneous station distribution. Comparing these horizontal and vertical errors to the mapped locations, the formal errors underestimate the actual horizontal and vertical errors between the possible

locations, no matter the crustal model used. Since the seismometers are mostly on land and do not encircle the offshore earthquakes, the derived locations have a horizontal bias towards the onshore stations, pulling the horizontal locations farther from the other possible locations than the formal calculated horizontal error. The vertical error is also dependent on the location of the stations, but is also heavily influenced by the V_p/V_s ratio. If there is a good V_p/V_s ratio estimate and a station above the source, then there will be an accurate estimate of depth and vertical error. In general, for an accurate vertical error estimate, the stations have to be within a distance on the surface that is less than the depth. For example, if the earthquake is about 20 km deep, there would ideally be seismometers recording the earthquake within 20 km of the epicenter.

Although the few offshore seismometers were within this desired distance of each earthquake, most of the seismometers were located on land, outside of the range of this distance. This bias towards the land stations pulls the vertical depths farther from the other possible locations than the formal calculated vertical error.

Even though the formal errors do not agree with the observed errors, they still are valuable in examining the uncertainty of the two crustal models. Although the thick crust model has lower RMS values compared to the thin crust model, the horizontal and vertical errors are generally higher than with the thin crust model. This is because of the geometrical factors that control accuracy. When OBS data are included, a wider range of azimuths between the source and the stations is available, which provides better control over the epicenter, and the distance to the closest station is smaller, providing better control over the depth.

Lastly, it is important to note that both of these crustal models are one-dimensional models being used to find locations in a three-dimensional crust. Both of these models are taken from a two-

dimensional model of the Cascadia Subduction Zone, as shown in Figure 1, which means that both models represent different sections of the subduction zone. One-dimensional models were used instead of two- or three-dimensional models due to the lack of consensus on a three-dimensional model for the entire region of Cascadia and the computational requirements for calculating hypocenters in more complex models. Using simple velocity models allowed us to vary the parameters systematically in order to gain a better understanding of the sensitivity of the solution to the various sources of error. While the exact locations of these three earthquakes are still not known, we have a better understanding of how the different crustal models affect the assumed locations of the earthquakes.

Chapter 5 – Future Research

More work is needed on these three earthquakes to better understand the relationship between crustal model and location, and to potentially decrease the bias and uncertainty due to uncertainties in velocity models. More combinations of stations need to be tested with all three earthquakes to explore the idea of having the stations positioned mostly in a thick region but the earthquake being in a thin part of the crust. Different combinations can also help explore the potential problem of having poor data at some stations. Fault plane solutions can also be looked at to find the fault mechanisms at work in this area. HYPO71 gave data for the fault plane solution; however, it was inconclusive. Going back and looking at this fault plane data and re-picking some of the arrival times will give more information about this area of the crust. The next step, after wrapping up this work in the one-dimensional models, will be looking at these earthquakes with three-dimensional models, which are more accurate due to the fact that the crustal structure varies dramatically both laterally and as a function of depth [2]. The last step will be to repeat all of this work for earthquakes located off the coast of Chile. The subduction zone in Chile has a structure similar to the Cascadia Subduction Zone, giving us another good analog of this relationship between crustal model and location in subduction zones.

References

- [1] Tréhu, A.M. Final report: The relationship between crustal structure and earthquake activity on the central Cascadia continental margin in 3D. *NEHRP grant G17AP00046* (2020).
- [2] Tréhu, A. M., Wilcock, W. S. D., Hilmo, R., Bodin, P., Connolly, J., Roland, E.C., & Braunmiller, J. The role of the Ocean Observatories Initiative in monitoring the offshore earthquake activity of the Cascadia subduction zone. *Oceanography* **31**, 104- 113 (2018).
- [3] Webb, S. C., Broadband seismology and noise under the ocean. *Reviews of Geophysics* **36**, 105-142 (1998).
- [4] Tréhu, A. M., Braunmiller, J., & Davis, E. Seismicity of the central Cascadia continental margin near 44.5° N: a decadal view. *Seismological Research Letters* **86**, 819-829 (2015).
- [5] Husen, S., & Hardebeck, J. L. Earthquake location accuracy, *Community Online Resource for Statistical Seismicity Analysis*, doi:10.5078/corssa-55815573 (2010).
- [6] Williams, M. C., Tréhu, A. M., & Braunmiller, J. Seismicity at the Cascadia plate boundary beneath the Oregon continental shelf. *Bulletin of the Seismological Society of America* **101**, 940-950 (2011).
- [7] Richardson, R. M., Prof., & Zandt, G., Prof. Inverse problems in geophysics GEOS 567[a set of lecture notes]. *University of Arizona, Tucson* (2009).

Appendix: Tables

Table 1

Station information, including name, latitude, longitude, elevation and calculated station delay times. Stations numbered 48 and above are OBSs while the rest are onshore stations.

Station Name	Latitude (degrees and minutes)	Longitude (degrees and minutes)	Elevation (m)	Station Delay Time (s)
OR01	44°52.17' N	123°59.86' W	218	0.09
OR02	44°50.69' N	123°52.00' W	468	0.19
OR03	44°32.20' N	123°54.67' W	288	0.12
OR04	44°50.78' N	123°34.78' W	793	0.32
OR05	44°51.13' N	123°26.1' W	130	0.05
OR06	44°40.62' N	124°0.12' W	239	0.10
OR07	44°39.48' N	123°47.36' W	192	0.08
OR08	44°39.97' N	123°38.29' W	228	0.09
OR09	44°40.66' N	123°30.45' W	320	0.13
OR10	44°40.41' N	123°18.96' W	471	0.19
OR11	44°23.57' N	124°2.78' W	97	0.04
OR12	44°25.10' N	123°54.26' W	116	0.05
OR13	44°23.50' N	123°44.27' W	76	0.03
OR14	44°32.35' N	123°41.20' W	111	0.04
OR15	44°24.78' N	123°23.34' W	242	0.10

OR16	44°12.10' N	124°2.64' W	599	0.24
OR17	44°13.44' N	123°50.87' W	374	0.15
OR18	44°19.80' N	123°31.99' W	386	0.15
OR19	44°13.30' N	123°35.86' W	569	0.23
OR20	44°12.44' N	123°25.78' W	320	0.13
OR21	44°1.45' N	124°2.93' W	49	0.02
OR22	44°12.44' N	123°52.86' W	195	0.08
OR23	44°0.52' N	123°48.33' W	349	0.14
OR24	44°6.66' N	123°39.38' W	337	0.13
OR25	44°3.09' N	123°36.74' W	425	0.17
OR26	44°0.80' N	123°24.82' W	281	0.11
OR27	43°55.22' N	123°10.14' W	343	0.14
OR28	43°52.49' N	122°52.90' W	629	0.25
OR29	43°51.00' N	124°4.79' W	121	0.05
OR30	43°48.99' N	123°53.12' W	354	0.14
OR31	44°20.19' N	123°59.57' W	266	0.11
OR32	44°19.79' N	123°47.46' W	93	0.04
OR33	43°49.68' N	123°28.00' W	351	0.14
OR35	44°24.62' N	123°35.71' W	315	0.13
OR48	44°40.07' N	124°44.96' W	-187	-0.12
OR49	44°39.07' N	124°30.57' W	-134	-0.09
OR50	44°21.08' N	124°30.50' W	-97	-0.06

OR51	44°4.10' N	124°43.47' W	-112	-0.07
OR52	44°3.66' N	124°26.72' W	-123	-0.08
OR53	44°4.37' N	124°58.44' W	-452	-0.30
OR54	44°26.13' N	124°43.55' W	-138	-0.09

Table 2

P- and S-wave arrival time picks for the June 28, 2012 earthquake event. The difference between the two pick times are also recorded.

Station Name	Polarity (up or down)	Arrival Hour (hr)	Arrival Minute (min)	P-wave Arrival Second (s)	S-wave Arrival Second (s)	Difference between S- and P-wave Arrival Times (s)
OR01	U	19	36	0.49	6.86	6.37
OR02	U	19	36	1.23	8.04	6.81
OR03	U	19	35	59.77	65.32	5.55
OR04	U	19	36	4.07	13.27	9.2
OR05	U	19	36	5.77	16.17	10.4
OR06	U	19	35	58.96	64.18	5.22
OR07	U	19	36	1.10	7.83	6.73
OR08	U	19	36	2.71	11.85	9.14
OR09	U	19	36	4.26	13.54	9.28
OR10	D	19	36	6.58	17.65	11.07
OR11	D	19	35	59.66	65.38	5.72

OR12	U	19	36	0.54	6.53	5.99
OR13	D	19	35	59.66	65.37	5.71
OR14	U	19	36	2.15	10.02	7.87
OR15	D	19	36	6.20	17.00	10.8
OR16	U	19	36	1.82	9.11	7.29
OR18	U	19	36	5.03		N/A
OR19	U	19	36	5.36	15.49	10.13
OR20	U	19	36	7.23	18.75	11.52
OR21	D	19	36	4.91	14.62	9.71
OR22	D	19	36	5.65	16.26	10.61
OR23	U	19	36	6.34		N/A
OR24	U	19	36	6.09	16.88	10.79
OR25	U	19	36	7.12	18.08	10.96
OR26	D	19	36	9.58	23.12	13.54
OR27	D	19	36	12.71	28.60	15.89
OR29	D	19	36	7.97	21.09	13.12
OR30	U	19	36	8.70	21.67	12.97
OR31	D	19	36	0.26	7.16	6.9
OR32	U	19	36	2.26	9.86	7.6
OR33	D	19	36	10.99		N/A
OR48	U	19	36	0.43	7.83	7.4
OR49	U	19	35	57.43	62.04	4.605

OR50	U	19	35	42.22		N/A
------	---	----	----	-------	--	-----

Table 3

Latitude, longitude, depth, uncertainty results, and number of stations used from HYPO71 for the June 28, 2012 earthquake event using all of the stations except for OR13 and OR50.

Crustal Model	Vp/Vs Ratio	Latitude (degrees and minutes)	Longitude (degrees and minutes)	Depth (km)	RMS	Horizontal Error	Vertical Error	Number of Stations Used
Thin	1.74	44°36.33' N	124°17.25' W	14.94	0.45	0.9	1.1	60
Thin	1.78	44°36.29' N	124°16.32' W	14.76	0.42	0.7	0.8	61
Thin	1.84	44°35.81' N	124°15.57' W	14.93	0.51	0.9	0.9	61
Thin	1.90	44°36.18' N	124°14.62' W	18.59	0.68	1.2	1.0	61
Thick/PNSN	1.74	44°37.28' N	124°20.47' W	28.12	0.37	0.8	1.0	60
Thick/PNSN	1.78	44°36.73' N	124°19.18' W	27.07	0.28	0.6	0.9	60
Thick/PNSN	1.84	44°35.92' N	124°17.28' W	23.31	0.30	0.6	1.0	61
Thick/PNSN	1.90	44°35.43' N	124°15.81' W	20.30	0.44	0.8	1.5	61

Table 4

Latitude, longitude, depth, uncertainty results, and number of stations used from HYPO71 for the June 28, 2012 earthquake event using all of the on-shore station data, except OR13, and none of the OBS data.

Crustal Model	Vp/Vs Ratio	Latitude (degrees and minutes)	Longitude (degrees and minutes)	Depth (km)	RMS	Horizontal Error	Vertical Error	Number of Stations Used
Thin	1.74	44°36.71' N	124°19.08' W	14.58	0.41	1.2	0.9	56
Thin	1.78	44°36.38' N	124°16.56' W	14.97	0.42	1.2	1.2	57
Thin	1.84	44°35.96' N	124°13.91' W	16.09	0.50	1.3	1.1	57
Thin	1.90	44°35.86' N	124°11.64' W	18.87	0.58	1.4	0.9	57
Thick/PNSN	1.74	44°37.53' N	124°22.23' W	26.67	0.30	1.0	1.5	56
Thick/PNSN	1.78	44°36.86' N	124°19.77' W	25.69	0.24	0.7	1.1	56
Thick/PNSN	1.84	44°36.19' N	124°16.59' W	24.76	0.26	0.7	1.0	57
Thick/PNSN	1.90	44°35.59' N	124°13.69' W	23.61	0.38	1.0	1.3	57

Table 5

P- and S-wave arrival time picks for the June 30, 2012 earthquake event. The difference between the two pick times are also recorded.

Station Name	Polarity (up or down)	Arrival Hour (hr)	Arrival Minute (min)	P-Wave Arrival Second (s)	S-wave Arrival Second (s)	Difference between S-and P-wave Arrival Times (s)
OR01	U	16	43	26.16	32.59	6.43
OR02	U	16	43	26.92	33.84	6.92
OR03	U	16	43	25.47	31.05	5.58
OR04	U	16	43	29.75	39.00	9.25
OR05	U	16	43	31.47	41.80	10.33
OR06	U	16	43	24.64	29.92	5.28
OR07	U	16	43	26.77	33.48	6.71
OR08	U	16	43	28.38		N/A
OR09	U	16	43	29.97	36.75	6.78
OR10	D	16	43	32.27	45.10	12.83
OR11	U	16	43	25.24	31.12	5.88
OR12	U	16	43	26.08	32.45	6.37
OR14	U	16	43	27.84	35.78	7.94
OR15	D	16	43	31.83	44.89	13.06
OR16		16	43		34.79	N/A

OR17	U	16	43	28.68	37.06	8.38
OR18	U	16	43	30.72	41.52	10.8
OR19	U	16	43	31.04	41.25	10.21
OR20	U	16	43	32.92	44.57	11.65
OR21	D	16	43	30.53	40.27	9.74
OR22	D	16	43	31.35	41.73	10.38
OR23	U	16	43	32.04	42.71	10.67
OR24	U	16	43	31.77	42.55	10.78
OR25	U	16	43	32.83	44.44	11.61
OR26	U	16	43	35.20	48.79	13.59
OR27	D	16	43	38.33	54.14	15.81
OR29	U	16	43	33.42	45.35	11.93
OR30	U	16	43	34.38	46.97	12.59
OR31	U	16	43	26.34	32.73	6.39
OR32	U	16	43	27.95	35.57	7.62
OR33	U	16	43	36.63	51.18	14.55
OB49	U	16	43	23.24	28.00	4.765
OB50	U	16	43	25.59	32.07	6.485

Table 6

Latitude, longitude, depth, uncertainty results, and number of stations used from HYPO71 for the June 30, 2012 earthquake event using all of the stations except OR09.

Crustal Model	Vp/Vs Ratio	Latitude (degrees and minutes)	Longitude (degrees and minutes)	Depth (km)	RMS	Horizontal Error	Vertical Error	Number of Stations Used
Thin	1.78	44°36.35' N	124°16.77' W	14.50	0.41	0.8	0.7	61
Thin	1.84	44°36.09' N	124°15.86' W	16.03	0.48	0.9	0.9	61
Thin	1.90	44°35.29' N	124°14.56' W	16.45	0.66	1.2	1.2	61
Thick/PNSN	1.78	44°36.97' N	124°18.81' W	28.44	0.24	0.5	0.7	59
Thick/PNSN	1.84	44°36.00' N	124°17.14' W	24.47	0.30	0.6	0.9	60
Thick/PNSN	1.90	44°35.28' N	124°16.04' W	21.53	0.44	0.8	1.4	61

Table 7

Latitude, longitude, depth, uncertainty results, and number of stations used from HYPO71 for the June 30, 2012 earthquake event using all of the on-shore station data, except OR09, and none of the OBS data.

Crustal Model	Vp/Vs Ratio	Latitude (degrees and minutes)	Longitude (degrees and minutes)	Depth (km)	RMS	Horizontal Error	Vertical Error	Number of Stations Used
Thin	1.78	44°36.51' N	124°17.83' W	14.81	0.40	1.1	1.1	57
Thin	1.84	44°35.84' N	124°15.30' W	16.25	0.49	1.3	1.0	57
Thin	1.90	44°35.41' N	124°13.04' W	18.57	0.61	1.6	1.0	57
Thick/PNSN	1.78	44°36.90' N	124°19.77' W	26.98	0.21	0.7	1.0	55
Thick/PNSN	1.84	44°35.93' N	124°16.92' W	24.57	0.28	0.9	1.2	56
Thick/PNSN	1.90	44°35.38' N	124°14.61' W	23.63	0.44	1.2	1.6	57

Table 8

P- and S-wave arrival time picks for the June 21, 2012 earthquake event. The difference between the two pick times are also recorded.

Station Name	Polarity (up or down)	Arrival Hour (hr)	Arrival Minute (min)	P-wave Arrival Second (s)	S-wave Arrival Second (s)	Difference between S- and P-wave Arrival Times (s)
OR03	D	15	57	15.075	23.235	8.16
OR08	U	15	57	18.665	29.355	10.69
OR09	U	15	57	19.975	32.065	12.09
OR11	D	15	57	13.145	19.925	6.78
OR12	D	15	57	14.545	22.255	7.71
OR17	D	15	57	15.825		N/A
OR18	U	15	57	19.165	30.555	11.39
OR20	D	15	57	16.505		N/A
OR21	D	15	57	15.995	24.825	8.83
OR22	U	15	57	17.63	27.9	10.27
OR23	D	15	57	18.27		N/A
OR29	U	15	57	17.945	28.935	10.99
OR30	U	15	57	19.69	31.14	11.45
OR32	D	15	57	15.92	24.65	8.73

Table 9

Latitude, longitude, depth, uncertainty results, and number of stations used results from HYPO71 for the June 21, 2012 earthquake event using all of the stations available, except OR20.

Crustal Model	Vp/Vs Ratio	Latitude (degrees and minutes)	Longitude (degrees and minutes)	Depth (km)	RMS	Horizontal Error	Vertical Error	Number of Stations Used
Thin	1.77	44°25.47' N	124°32.70' W	14.82	0.23	1.2	1.2	24
Thin	1.78	44°25.30' N	124°32.17' W	15.82	0.22	1.1	0.8	24
Thin	1.84	44°24.40' N	124°28.13' W	20.05	0.22	1.0	0.9	24
Thin	1.90	44°23.35' N	124°23.57' W	21.57	0.25	1.2	0.9	24
Thick/PNSN	1.77	44°26.21' N	124°34.46' W	30.53	0.25	1.4	2.1	24
Thick/PNSN	1.78	44°25.79' N	124°32.69' W	31.93	0.24	1.4	2.1	24
Thick/PNSN	1.84	44°25.32' N	124°29.18' W	30.64	0.21	1.1	1.4	24
Thick/PNSN	1.90	44°23.95' N	124°24.32' W	31.41	0.24	1.3	1.5	24

Table 10

Latitude, longitude, depth, uncertainty results, and number of stations used from HYPO71 for the June 21, 2012 earthquake event using the stations depicted in Figure 1.12.

Crustal Model	Vp/Vs Ratio	Latitude (degrees and minutes)	Longitude (degrees and minutes)	Depth (km)	RMS	Horizontal Error	Vertical Error	Number of Stations Used
Thick/PNSN	1.78	44°24.87' N	124°31.27' W	33.41	0.08	1.5	2.0	6

Table 11

Latitude, longitude, depth, uncertainty results, and number of stations used from HYPO71 for the June 21, 2012 earthquake event using the stations depicted in Figure 1.15.

Crustal Model	Vp/Vs Ratio	Latitude (degrees and minutes)	Longitude (degrees and minutes)	Depth (km)	RMS	Horizontal Error	Vertical Error	Number of Stations Used
Thick/PNSN	1.78	44°25.71' N	124°33.29' W	29.57	0.19	1.6	2.6	15

